LAWRENCE
LIVERMORE
NATIONAL
LABORATORY

LLNL-JRNL-661048

One-dimensional particle simulations of Knudsen-layer effects on D-T fusion

B. I. Cohen, A. M. Dimits, G. B. Zimmerman, S. C. Wilks

September 24, 2014

Physics of Plasmas

Disclaimer

One-dimensional particle simulations of Knudsen-layer effects on D-T fusion

Bruce I. Cohen, Andris M. Dimits, George B. Zimmerman, and Scott C. Wilks
Lawrence Livermore National Laboratory, Livermore, CA 94551

Abstract

Particle simulations are used to solve the fully nonlinear, collisional kinetic equation describing the interaction of a high-temperature, high-density deuterium-tritium plasma with absorbing boundaries, a plasma source, and the influence of kinetic effects on fusion reaction rates. Both hydrodynamic and kinetic effects influence the end losses, and the simulations show departures of the ion velocity distributions from Maxwellian due to the reduction of the population of the highest energy ions (Knudsen-layer effects). The particle simulations show that the interplay between sources, plasma dynamics, and end losses results in temperature anisotropy, plasma cooling, and concomitant reductions in the fusion reaction rates. For the model problems and parameters considered, the particle simulations show that the Knudsen-layer modifications to the velocity distribution function do not significantly affect the fusion reaction rates if the local densities and bulk temperatures are used to evaluate the thermal fusion reaction rates.

I. INTRODUCTION

In a fusion plasma the interplay between kinetic effects and absorbing boundaries can reduce the fusion reaction rates relative to the reaction rates that a Maxwellian velocity distribution supports due to the loss of high-energy ions.[1-4] The reduction in fusion reaction rates can be understood on the basis of the following rationale. The high-energy ions are less collisional than the lower energy ions because their characteristic collision rates scale as $\nu \propto \mathrm{v}^{-3}$, and their collisional mean-free-paths scale as $l_{mfp} = \mathrm{v}/\nu \propto \mathrm{v}^4$ so are much longer than those of the thermal particles, where v is the particle speed, ν is the collision frequency at this speed, and l_{mfp} is the collisional mean free path. Thus, the high-energy ions have a higher relative probability of impinging on a bounding surface than do the thermal particles. If the bounding surface absorbs

impinging ions, then the neighboring plasma velocity distribution, which in thermal equilibrium would be a Maxwellian, will be depleted at higher energies relative to a Maxwellian and give rise to a Knudsen-layer (KL) velocity distribution [3,4]. Because the cross-section for deuterium-tritium nuclear fusion steadily increases with increasing energy up to a peak value near ~70 keV, which is a much larger energy than the mean thermal energies in the inertial fusion scenarios considered here, the loss of high-energy ions in the KL velocity distribution function reduces the total fusion reactivity.[5,6]

Here we report the study of KL effects on fusion reactivity using particle-in-cell simulations of a weakly coupled, deuterium-tritium plasma interacting with an absorbing boundary at both sides of the system and a planar source on the left. The particle simulations model a system that has one spatial dimension with a Cartesian coordinate z, and three dimensions in velocity $\{v_x, v_y, v_z\}$. Conventional particle-in-cell and Monte Carlo methods are employed.[7,8] The simulation of KL effects on fusion in a one-dimensional system solving the fully nonlinear collisional kinetic equation with a spatially localized source at one end of the system and absorbing boundaries (or partly reflecting and rethermalizing boundary conditions) differentiates this study from the calculations reported in Ref. 3, which solved linearized kinetic equations in velocity variables and mocked up losses to a bounding surface without including any true spatial dependence. The calculations in Ref. 4 linearize the kinetic equation, but include spatial dependence.

In our particle simulations, deuterium (D) and tritium (T) ions are represented as equally weighted particles; and the collisions conserve particle number, momentum, and energy. Charge-neutralizing electrons are modeled as a fluid with a Boltzmann response to electrostatic fields in some of the simulations.[7,8] D-D, T-T, and D-T Coulomb collisions are represented as pairwise collisions using the algorithms of Takizuka and Abe,[9] and Nanbu.[10] We used the ICEPIC particle code developed by R. J. Procassini.[11] A fusion subroutine was added based on the models for the fusion of Maxwellian velocity distributions and for more general velocity distributions as given in Bosch and Hale's paper.[5]

This paper is organized as follows. The methodology for the simulations including verification tests is described in Sec. II. Simulation results examining the

Knudsen-layer effect on fusion reaction rates are presented in Sec. III. A matrix of simulations was undertaken examining the effects of the plasma source and initial temperature, the reflectivity (albedo) of the bounding surface, the presence of a 0.001 concentration of fully ionized copper ions, the presence of fusion alphas, slowing down of the ions on fluid electrons, the inclusion of the self-consistent ambipolar electric field, the artificial suppression of all collisions, and increasing the strength of the plasma source. Comparisons are made between the results of particle and simplified hydrodynamic simulations.

The principal conclusions (Sec. IV) are that the interplay between the plasma source, absorbing walls, the plasma dynamics, and kinetic effects determine the development of the spatial profiles of the plasma temperatures T_z=m(<v_z^2>-<v_z>^{2}) and $T_\perp = \frac{1}{2} m < v_x^2 + v_y^2 >$ associated with the axial and perpendicular velocity distributions, the plasma densities, the mass motion away from the plasma source, and the resulting fusion reaction rates. We observe cooling of the plasma as a function of increasing distance from the plasma source, and an anisotropy often develops with $T_z < T_\perp$. Hydrodynamic simulations show qualitative agreement with the particle simulations for the steady-state plasma profiles. Moreover, for the parameters used in our simulations, number densities ~10^{24} cm^{-3} and temperatures 4 – 12 keV, the Knudsen-layer effects on the velocity distributions are observed to occur at energies much greater than the Gamow energy where the fusion reactivity peaks.[6] The fusion reactivities of the D-T plasma with general velocity distributions using the kinetic model of Bosch and Hale[5] are matched well by the fusion reactivities using a thermal model for a Maxwellian velocity distribution with the local density and temperature defined by

$$T_2 \equiv \tfrac{1}{3} m \left[< v_z^2 > - < v_z >^2 + < v_x^2 > + < v_y^2 > \right]. \qquad (1)$$

T_2 evolves to be less than the initial temperatures of the system and the planar source. The cooling is due both to end losses and to the partitioning of the axial kinetic energy between the mean axial drift energy and the axial temperature. Moreover, if the deuterium and tritium densities evolve so that they are less than the initial densities, then the fusion reaction rates are substantially reduced relative to the initial reaction rates. .

II. METHODOLOGY

The particle code ICEPIC[11] was used to perform simulations of a D-T plasma in one Cartesian spatial dimension with a planar source at the left boundary (z=0), absorbing boundary at the left side, and an absorbing or partially reflecting wall at the right boundary (z=L). Plasma ions are represented as particles in three velocity dimensions. The planar source at the left boundary is constructed by randomly sampling an axial velocity distribution function given by $\propto v_z \exp(-v_z^2/2v_{th}^2)$ for v_z>0 and a perpendicular velocity distribution $\propto v_\perp \exp(-v_\perp^2/2v_{th}^2)$, both of which are readily integrated to obtain the cumulative distribution functions. The form of the axial velocity distribution is chosen to offset the natural $1/v_z$ reduction in the spatial number density of the injected particles as they stream away from the source so that the resultant velocity distribution at finite z after a transit time of the bulk of the velocity distribution in a collisionless plasma will tend toward a half-Maxwellian locally in the volume. The $v_\perp$ pre-factor in the perpendicular velocity source is due to the two-dimensional phase-space area element. In simulations with finite reflectivity and rethermalization from the right boundary, a similar source is used at z=L, but the injected ions have v_z<0 and the rethermalization source temperature is an adjustable parameter. The planar source injection rate per unit area is chosen empirically to approximately balance the loss rates to the end walls after transients relax:

$$S = dN/dt = 0.4\left(1. - 0.75R\right)N_0 v_{th}/L \qquad (2)$$

where R is the reflectivity of the bounding surface at the right side of the system, L is the length of the system, N_0/L is the number density of simulation particles, and $v_{th}=(T/m)^{1/2}$ is the thermal velocity corresponding to the temperature T.

Ion-ion Coulomb collisions are modeled using the pairwise scheme introduced by Takizuka and Abe[9] and extended to larger time step (aggregating multiple small-angle collisions) by Nanbu.[10] In these algorithms equally weighted particles are paired, and the relative velocity vector is scattered through an angle. These algorithms algebraically conserve particle number, momentum, and energy. Coulomb collisions of the ions with fluid electrons are modeled with a Langevin equations collision operator.[12,13] The Langevin equations collision operator does not conserve energy nor momentum, but

energy and momentum conservation can be patched with scaling and shifting of the particle velocities after the collisions are computed.[12] The accuracy of the Takizuka and Abe, and Langevin equations collision models with respect to time step was investigated for a few test cases involving like and unlike species collisions in Ref. 13. Several of the test cases in Ref. 13 were employed to verify the accuracy of the collision algorithms in ICEPIC as part of this study: preservation of a Maxwellian; conservation of momentum and energy for the pairwise collision algorithms; relaxation of a weak temperature anisotropy; and slowing down of a relative electron-ion drift. These collision algorithms use lowest order Euler-Maruyama integration schemes, and good accuracy with respect to time step is obtained when the product of the characteristic collision frequency and the time step is $\leq O(10^{-2})$.[13] The Monte Carlo aspect of these collision algorithms introduces a statistical component to the accuracy considerations. [13,14]

In order to compute D-T fusion in the simulations, the calculation of the D-T kinetic fusion cross-section σ based on Equations (8) and (9), and Table IV in Bosch and Hale[5] was added into a new subroutine in ICEPIC. Deuterium and tritium ions are randomly paired within each spatial cell using the same logic as the Takizuka and Abe pairing algorithm,[9] and fusion reactions are summed over randomly sampled D-T pairs in each spatial cell to model general velocity distribution functions that may have spatial gradients. The cross-section σ is evaluated using the energy of the deuterium ion evaluated in the rest frame of the tritium ion. We also coded Eqs. (12-14) in Bosch and Hale[5] to model the thermal D-T fusion probabilities $\langle\sigma v\rangle$ averaged over a Maxwellian assuming the deuterium and tritium are in thermal equilibrium. The thermal fusion reaction rates then depend only on the local temperature and the product of the densities of the deuterium and tritium. We checked the implementation of the thermal Maxwellian fusion reaction rates by recovering the thermal reaction rates in Table VIII in Ref. 5 for the temperatures of interest in this study (to better than 1% accuracy).

To verify the implementation of the kinetic D-T fusion reaction rates and to test the statistical accuracy of the particle representation of the velocity distributions and its influence on the fusion reaction rates, we undertook simulations with an initial Maxwellian, reflecting boundary conditions, and D-D, T-T, and D-T Coulomb collisions. Figure 1 shows the results for the ratio of the kinetic fusion reaction rate to the thermal

Maxwellian fusion reaction rate as functions of position at fixed time and functions of time averaged over the system with 100 cells for 400, 900, and 10^4 ions of each species per spatial cell. We observe that the ratios of the kinetic to thermal fusion rates converge to unity from below as the particles per cell increase. We attribute this to the improved resolution of the velocity distributions with increasing numbers of particles. The statistical accuracy of the fusion ratio for 10^4 ions of each species per spatial cell in space is ~2% (based on the computed standard deviation of the kinetic fusion rates) and, when averaged over the 100 cells, improves by an order of magnitude. The simulations described in the next section employed 10^4 ions of each species per spatial cell.

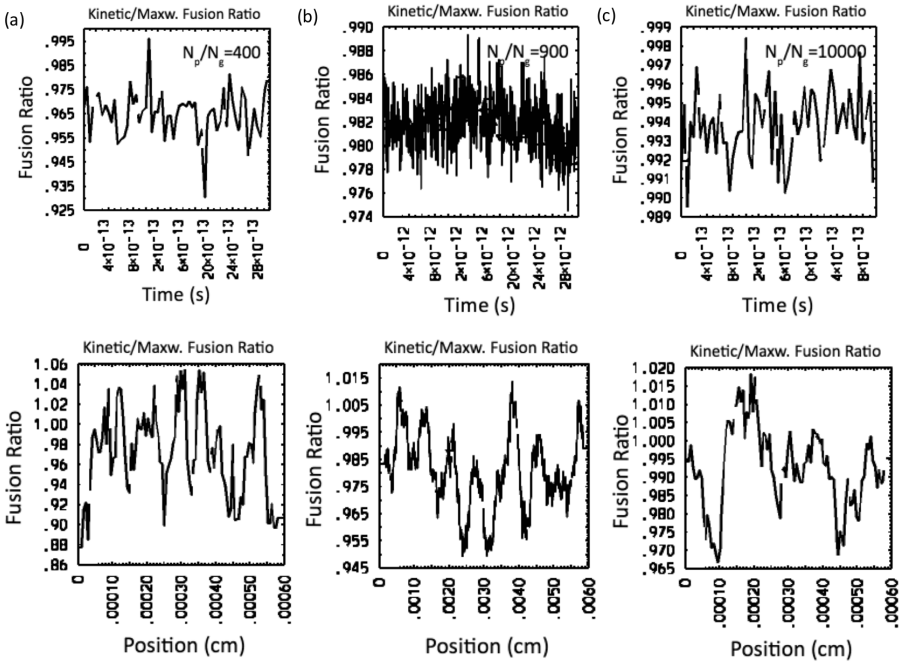

Figure 1. Convergence of kinetic fusion reactivity with respect to particle statistics: (a) 400, (b) 900, (c) 10^4 ions of each species per spatial cell. Ratios of the kinetic fusion rate divided by the thermal Maxwellian fusion rate averaged over N_g=100 spatial cells as functions of time are plotted on top and as functions of position at a fixed time on the bottom. Note that the time series in (b) is 10× longer than those in (a) and (c).

III. D-T FUSION SIMULATIONS

A set of simulations was performed to explore the Knudsen-layer effects on D-T fusion. We first describe the base case in detail. We follow this with a summary of the results of other simulations in which various parameters and physics aspects were varied.

A. Base-case simulation

The base case has the following parameters: Knudsen number $N_k=\ell_{mfp}/L=(v_{th}/\nu)/L$ =0.1 for a thermal deuterium ion, T_0=9 keV, number densities $n_0=1\times10^{24}$ cm^{-3} (D and T), ν is the collision frequency of a thermal deuterium ion, 10^4 particles/cell per ion species, L=3 micron, N_g=100 cells (Δz=0.03 micron), for 3 ps and 30 ps durations, where v is the total effective deuterium collision frequency, ℓ_{mfp} is the collisional mean free path, and the thermal velocity is $v_{th}=(T_I/m_D)^{1/2}$. The boundary condition at the right side of the system is completely absorbing, but in other simulations we have varied the reflectivity of the right side boundary. The left side boundary is fully absorbing in the simulations discussed in this section, and there is a planar source at the left side for D and T at 9 keV.

The characteristic collision frequency of specie i on j, ν_{ij}, is defined by

$$\nu_{ij}=\frac{4\pi n_j q_i q_j}{m_i^{1/2}T_i^{3/2}}\ln\Lambda_{ij} \tag{3}$$

where $\ln\Lambda_{ij}\approx5$ for the base case, and $\nu_{DD}\sim\nu_{TT}\sim\nu_{DT}\sim10^{12}$ s^{-1}. With these collision frequencies we use a time step $\Delta t=10^{-14}$s, and the total effective deuterium collision frequency is $v=\nu_{DD}+\nu_{DT}\sim2\text{x}10^{12}$ s^{-1}. For simulation durations τ= 3 ps and 30 ps, $v\tau$= 6 and 60. The deuterium thermal velocity at 9 keV is $v_{th}=6.5\times10^7$ cm/s, and ℓ_{mfp}=0.3 microns = 0.1L for a thermal deuterium in the presence of D-D and D-T collisions. We note that the collision frequency for deuterium ions with $v/v_{th}>1$ scales as $\nu(v_{th})\ (v_{th}/v)^3$, and the mean free path scales as $\ell_{mfp}(v_{th})\ (v/v_{th})^4$. A collisionless thermal deuterium ion traverses $v_{th}\tau$= 1.9 microns over 3 ps, which increases linearly with v/v_{th}. If we use a random walk argument for the expected spatial diffusion with step size $\Delta x\sim v\Delta\tau$ and time step $\Delta\tau\sim1/\nu$, then the spatial diffusion coefficient is $D\sim\langle\Delta x^2\rangle/\Delta\tau\sim v^2/\nu$. An estimate of the collisional diffusion of a thermal deuterium over τ=3 ps is then given by $(v_{th}^2\tau/v_{th})^{1/2}\sim0.8$ micron, and the collisional diffusion over 3 ps for a deuterium ion with $v/v_{th}>1$ scales as $(v/v_{th})^5(v_{th}^2\tau/v_{th})^{1/2}\sim(v/v_{th})^5\times0.8$ micron.

The simulation results for the base case with duration 30ps are shown in Figures 2-5. Figure 2 shows the spatial profiles after 30 ps for the deuterium and tritium number densities, mean flows $<v_z>$, and axial and perpendicular temperatures as functions of axial position. The profiles of the two ion species follow one another closely. The ion spatial profiles and fusion rates are effectively in steady state after 20-25 ps. The injection at z=0 of a half-Maxwellian leads to an average ion drift $<v_z>\sim 0.5v_{th}$ at steady state, where v_{th} is the initial thermal velocity. In the collisionless limit the average velocity $<v_z>=(2/\pi)^{1/2}v_{th}$ is higher than in the collisional case, and the half-Maxwellian would have a temperature relative to the mean drift given by $T_z=(1-2/\pi)mv_{th}^2=3.27$ keV in the collisionless case. Hence, the injection of a half-Maxwellian at z=0 and the absorbing boundary conditions naturally lead to a temperature anisotropy between T_z and $T_\perp$; and the half-Maxwellian in the collisionless limit (Case 8) would have a composite temperature $T_2=(3-2/3\pi)T_0/3=7.1$ keV for T_0=9 keV. In the collisional base case, the kinetic energy associated with the mean drift is less than in the collisionless case; and the axial temperature is higher. We observe T_z=7.0 keV, $T_\perp$=7.8 keV and T_2=7.5 keV at steady state, so that the composite temperature T_2 is higher in the collisional case than in the collisionless case. The collisions moderate the temperature anisotropy at the expense of cooling $T_\perp$. At steady state in the base case, the pressure gradient is negative; and $<v_z>$ is an increasing function of z, while the ion number densities n are decreasing functions of z so that the flux is relatively constant (Fig. 2). In these simulations the end loss of the higher axial velocity ions also contribute to cooling the plasma. Hydrodynamic rarefactions in the plasma also can contribute to some initial cooling of the plasma as transients relax.[15] However, the steady-state plasma conditions are mostly determined by the balance of the plasma sources, the plasma dynamics, and the absorbing boundary conditions.

The plasma sources, flows, and absorbing boundary conditions lead to lower temperatures and lower ion densities than those in the initial state. This leads to a substantially reduced fusion reaction rate as compared to the initial fusion rate (Fig. 5). The fusion rates shown in Figs. 5 and 6, and tabulated in Table 2 are in units of number of reactions/ (ps cm^2 Δz). The fusion rates in Fig. 5a have been temporally averaged over ~16 time steps (simple lag average). The unsmoothed, spatially local kinetic fusion

reaction rates exhibit a standard deviation that is approximately 4% of the locally spatially smoothed instantaneous fusion reaction rates. The volume-averaged fusion reaction rates have not been smoothed in time. To isolate the effects on the fusion reaction rates of the change in the velocity distribution excluding changes in the densities, we compute the thermal Maxwellian fusion reaction rates using the local (in time and space) D-T density at the initial and source temperature T_1=9 keV (Fig. 5). We observe that the kinetic fusion reaction rates are substantially reduced from the thermal Maxwellian fusion reaction rates using T_1, viz., the kinetic fusion reactions rates at 30 ps are 0.57 of the thermal Maxwellian reaction rates for a Knudsen number N_k=0.11 (adjusted for the ion densities and temperatures at 30 ps). Interestingly, this reduction is similar in magnitude to the fusion reduction in the linearized kinetic slab calculation 0.62 at 9 keV for N_k^{cav} =0.12 shown in Fig. 5 of Ref. 4.

We observe in the plots of the axial velocity distribution functions for the deuterium ions at z= 0.*2L* and 0.*9L* in Fig. 3 that the ions have acquired a net drift toward the absorbing boundary, a slight left-right asymmetry (probably a remnant of the half-Maxwellian source), and a reduction of the highest energy ion population that is more pronounced as the particle energy increases. This depletion of the most energetic ions is a characteristic feature of the KL velocity distributions.[3,4] For axial velocities $|v_z-v_{pk}|<3v_{th}$ (using the intial/source thermal velocity v_{th} and v_{pk} is defined by v_z where $f(v_z)$ peaks), $f(v_z-v_{pk})$ in Fig. 3 is reasonably well fit by a Maxwellian at the reduced temperature ~7 keV, while the perpendicular velocity distribution (Fig. 4) is slightly hotter ~8 keV (but cooler than the initial/source 9 keV). A good estimator of the kinetic fusion rate is obtained when we re-compute the thermal Maxwellian fusion rate using the local temperature T_2 in Eq.(1) and the local densities (Fig. 5).

That the thermal Maxwellian fusion rate using the local density and temperature T_2 is a good approximation to the kinetic fusion calculation is a consequence of the following factors. As already observed the perpendicular velocity distribution is observed to be close to a Maxwellian (albeit at a lower temperature than the intial/source temperature), and the axial velocity distribution function is close to a drifting Maxwellian for $|v_z-v_{pk}|<3v_{th}$. For an isotropic Maxwellian the fusion reaction rates peak at the Gamow energy[6]

$$\varepsilon_{Gp} = \left(\varepsilon_G / 4T\right)^{1/3} T, \quad \varepsilon_G = 1183\,\mathrm{keV} \tag{4}$$

For temperatures 7-10 keV, ε_{Gp}~$3T$; and most of the fusion reactivity comes from the interval T to $5T$ in energy based on a saddle-point integration.[6] For a weak anisotropy, the energy $5T$ corresponds to $\left|\mathrm{v}_z - \mathrm{v}_{pk}\right| \sim \left(10/3\right)^{1/2} \mathrm{v}_{th}$ and $(\mathrm{v_x},\mathrm{v_y}) \sim \left(10/3\right)^{1/2} \mathrm{v}_{th}$. Thus, the most active energy interval for fusion falls within the range of energies for which the observed velocity distribution is close to a Maxwellian.

We have also performed simplified Lagrangian hydrodynamic simulations[16] in one Cartesian spatial dimension to compare to the particle simulation of the base case. The hydrodynamic simulation has the same *net* injected mass flow into the plasma at z=0, an absorbing boundary condition at z=L, the same plasma temperature and density values at z=0 as in the particle simulation to be used as boundary conditions in the hydrodynamic simulation, and includes Braginskii viscosity in the momentum and energy balance equations.[16] At z=L fluid mass, momentum and energy are removed a rate given by the product of the local number density and axial fluid velocity. There is no ion heat conduction included. The hydrodynamic simulations use an average DT ion and scalar temperature and pressure. We force the hydrodynamic simulations to use the same value $\ln\Lambda$=5 as in the particle simulation. Like the particle simulation, the hydrodynamic simulation density decreases as the plasma flows toward z=L. The fluid velocity increases away from the source at z=0 and approaches sonic near z=L. The mass flux density is approximately constant in steady state; and the temperature and pressure decrease away from z=0. The decreases in density and temperature away from the plasma source at z=0 have obvious consequences in reducing the fusion reaction rates. The gradients in the hydrodynamic simulations are steeper for the density and fluid velocity than in the particle simulation, but for increased viscosity the hydrodynamic simulations yield flatter profiles. Recall that the viscosity coefficient is inversely proportional to the collisionality. The plasma profiles from the hydrodynamic simulations are shown in Fig. 6 after 30 ps. Like the particle simulation, the hydrodynamic simulation arrives at a steady state after 20-25 ps. Overall there is qualitative agreement between the hydrodynamic and particle simulations. It should be kept in mind that the hydrodynamic simulation model is much simplified and is justified only in the limit of

very short collisional mean free path, which is not well satisfied for a system with length equal to 10x the collisional mean free path of a thermal ions.

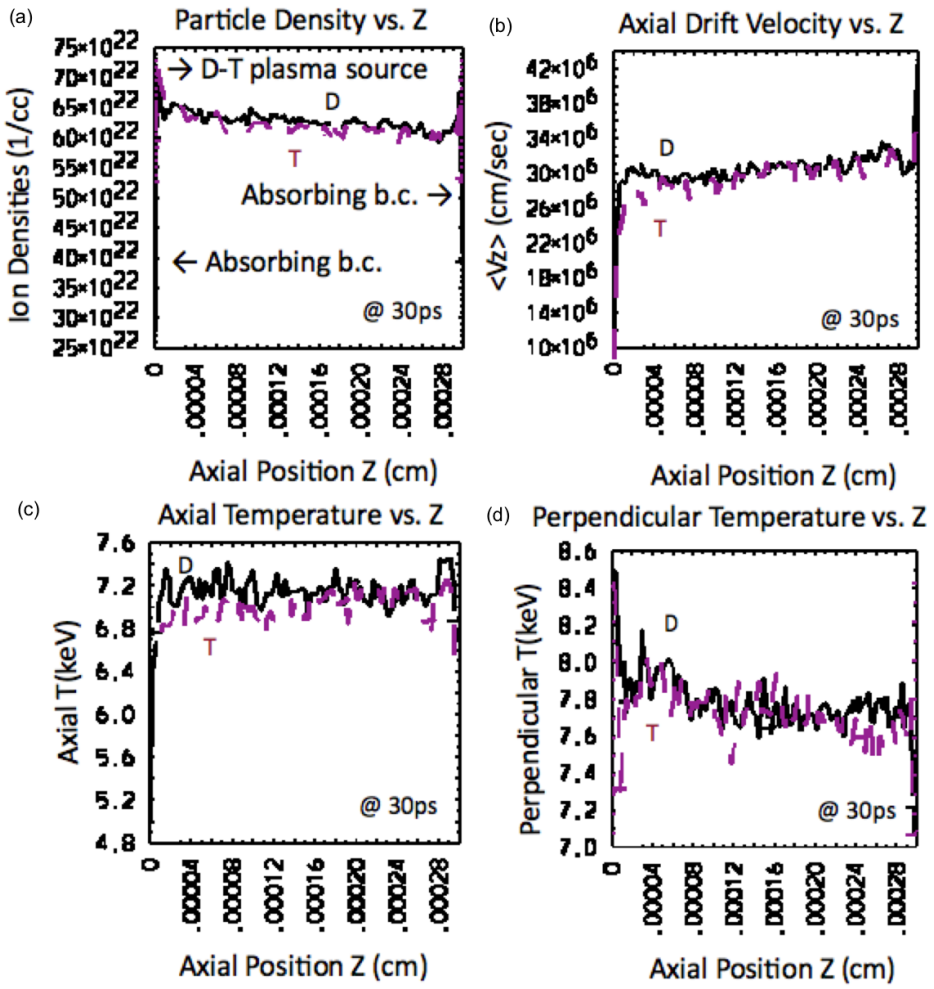

Figure 2. Plasma profiles for deuterium (black solid) and tritium (magenta dashed) number densities, axial drift velocities, axial and perpendicular temperatures as functions of axial position *z* at 30ps.

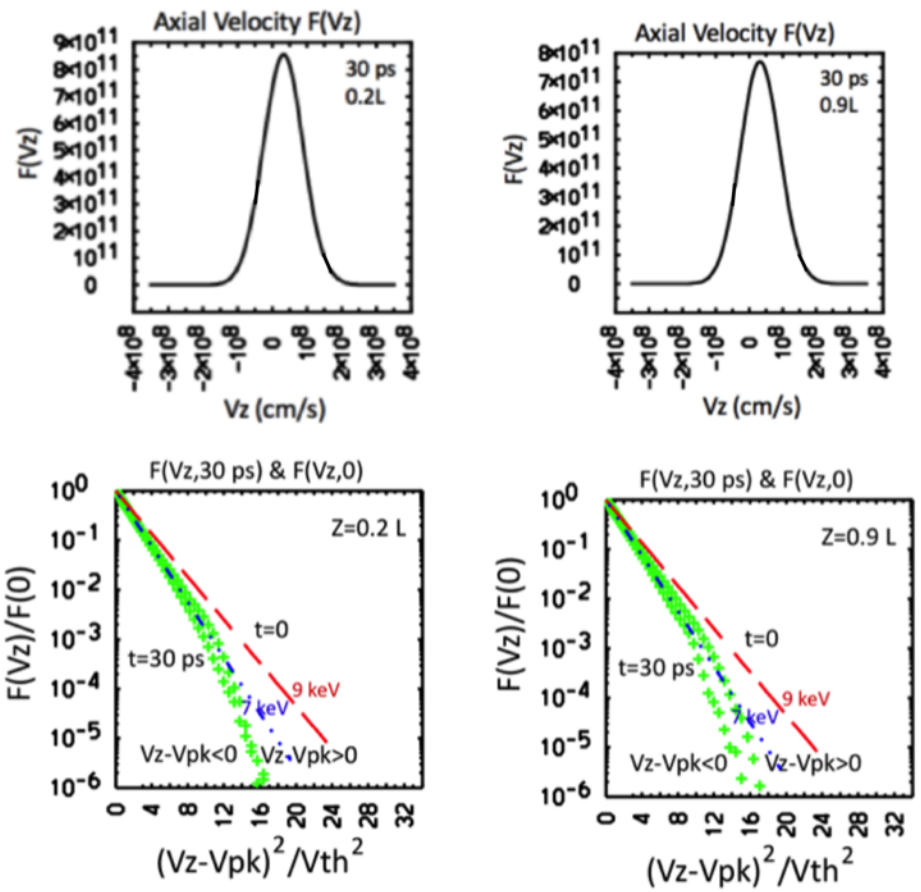

Figure 3. Axial velocity distribution functions at 30 ps as function of axial velocity (top) and $(v_z\text{-}v_{pk})^2/v_{th}^2$ (bottom) at z=0.2L and z=0.9L.

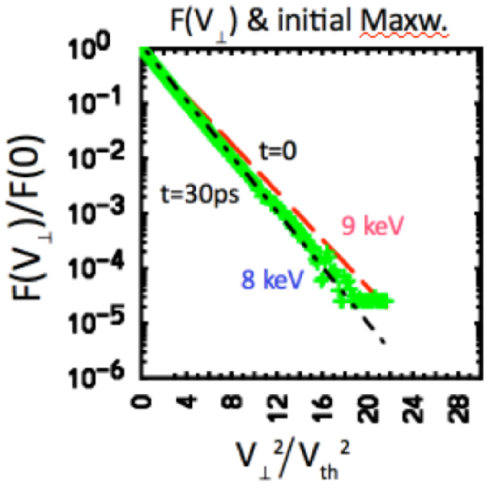

Figure 4. Perpendicular velocity distribution functions at 30 ps as a function of $v_\perp^2 / v_{th}^2$ integrated over the volume.

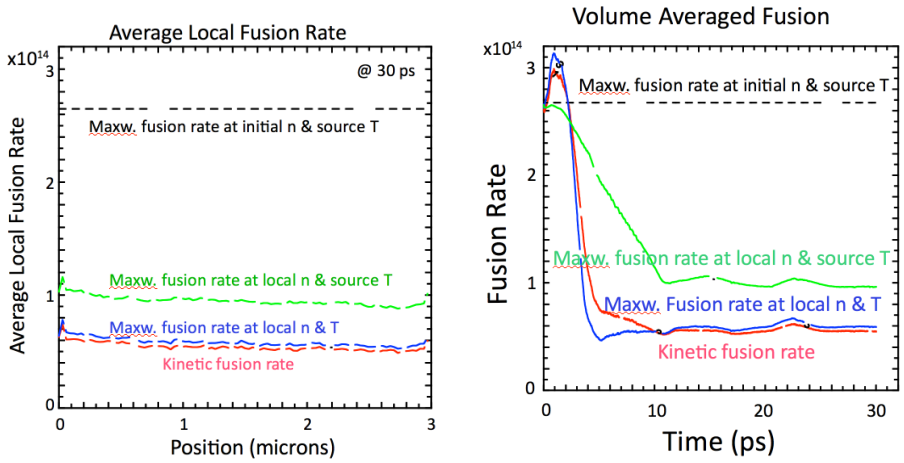

Figure 5. (a) Average local fusion rates as functions of position and (b) volume-averaged fusion rates as functions of time.

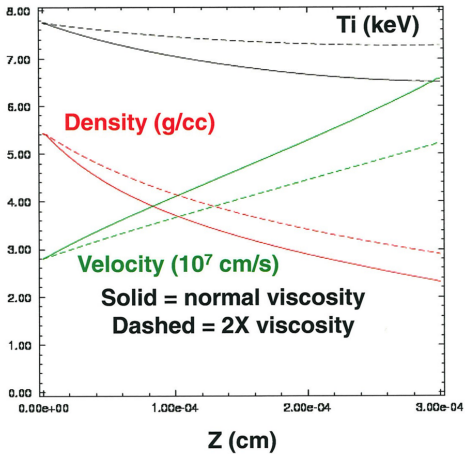

Figure 6. Results from two one-dimensional hydrodynamic simulations. Ion temperature (Ti), mass density, and fluid velocity vs. position *z* at 30 ps.

B. Suite of simulations

A suite of simulations was undertaken in which plasma conditions and boundary conditions were varied. Simulations for 3 ps and 30 ps were performed. Conditions and results are summarized in Tables 1 and 2 for the 30 ps simulations. The temperatures, $<v_z>$ at $z=L/2$, and the effective Knudsen numbers using the volume-averaged local densities and temperatures T_2 at 30 ps are tabulated in Table 2. Results are compared to those from the base case. In Table 2 we also tabulate the volume-averaged kinetic fusion reaction rates, and the ratios of the kinetic fusion rates to the thermal Maxwellian fusion rates using the local ion densities and either the initial/source temperature T_1 or the local temperature T_2. T_1=9 keV in Cases 1, 3, 5-8, and 11 while T_1=4 keV in Case 2; T_1=2 keV in Case 9; and T_1=12 keV in Case 2. In Case 4 the planar sources at left and right boundaries are at different temperatures, 9 keV and 4 keV, respectively; and it is not meaningful to define T_1. In Figure 7 we show the computed fusion reaction rates at z=0.2L, 0.5L, and 0.9L, and the volume-averaged rates for both the 3 ps and 30 ps simulations. In general, the results show that when the conditions lead to hotter and denser D-T plasmas, the computed fusion reactions rates increase. When the conditions lead to more collisional plasmas, the Knudsen number N_k is reduced; and the KL modification to the velocity distribution function is decreased. Generally, the computation of the thermal Maxwellian fusion reaction rates using the local density and the intial/source temperature T_1 significantly over-predicts the kinetic fusion reaction rates. The computation of the thermal Maxwellian fusion reaction rates using the local density and the local temperature T_2 gives improved estimates of the kinetic fusion reaction rates over three orders of magnitude in fusion rates.

The various cases in Tables 1 and 2 explore the sensitivity of the KL effects on the plasma evolution and the fusion reaction rates with respect to varying boundary conditions and plasma properties. Case 1 described in the previous sub-section is the base case. Case 2 is colder and is thus a more collisional plasma. The effective Knudsen number is reduced to N_k=0.024 The value of $<v_z>$ in Case 2 is reduced by O(1/2) relative to that in the base case, but the density is similar. The KL effects on $f(v_z)$ are much weaker, and there is very little temperature anisotropy. With the colder ion temperatures and the strong dependence of the fusion cross section on temperature, the fusion reaction

rate in Case 2 is an order of magnitude smaller than in the base case. In Case 3 the boundary condition at the right side is changed to 50% reflecting with the reflected ions rethermalized by a planar source at 9 keV. The plasma temperatures in Case 3 are slightly lower than in Case 1; $<v_z>$ is much reduced; but the density is higher (particularly near $z=L$). In consequence the kinetic fusion rate is higher in Case 3 than in Case 1. The KL effects on $f(v_z)$ are much weaker than in Case 1, and $T_\perp$ is slightly smaller than T_z. In Case 4 the right side boundary is 50% reflecting with rethermalization at 4 keV, while the source at $z=0$ remains at 9 keV. Case 4 evolves to a much colder plasma than in Cases 1 and 3, has a smaller $<v_z>$, less end loss than in Case 1, and higher density. The KL effects on $f(v_z)$ are much weaker in Case 4 than in Case 1. The densities in Case 4 are higher, but the temperatures are substantially lower than those in the base case, which leads to a lower fusion reactivity.

In Case 5 fully ionized Cu at 9 keV is introduced initially and with a planar source at z=0 at a 0.001 relative concentration compared to the deuterium and tritium. With this density and charge state $Z=29$, the collision rate of deuterium or tritium on Cu is comparable to $\nu_{DD,}$ ν_{DT}, and ν_{TT}. Thus, the inclusion of the Cu increases the deuterium and tritium collisionality by ~50% and decreases the Knudsen number to ~0.07 The plasma is more collisional and has a somewhat higher resulting density, and the end losses are decreased relative to Case 1. The temperatures in Case 5 are similar to those in Case 1, and the kinetic fusion reactivity is 20% higher due to the higher ion densities. The KL effects on $f(v_z)$ in Case 5 are weaker.

In Case 6 we add ion-electron collisions (primarily ions slowing on the electrons) and the computation of the self-consistent ambipolar electric field from the solution of Poisson's equation with fluid electrons modeled by a Boltzmann response. For purposes of the collisions the electrons are given a uniform density equal to the sum of the charge-weighted sum of the initial ion densities and an electron temperature T_e equal to the initial ion temperature 9 keV. The Langevin equations model for ion collisions with fluid electrons employed here does not allow changes in the electron fluid. For these parameters the collisional slowing down rates of the ions are much smaller than the ion-ion collision rates. With fluid electrons and Debye length $5\text{x}10^{-8}$ cm $<<\Delta z$, the sheaths at $z=0$ (source sheath) and $z=L$ cannot be resolved.[17] Sheath drops $\left|\Delta e\phi / T_e\right| < O(1)$ would be

expected,[17] and $e\phi / T_e \sim \ln \sum_s Z_s n_s / n_{0e}$ in the volume, where n_s is the spatially local ion number density and n_{0e} is equal to the time-dependent, volume-averaged, and charge-weighted ion number density. With little variation of the ion densities, the electric fields within the volume are weak and have little effect on the ion dynamics. There is no obvious evidence of microinstabilities accompanying the inclusion of the ambipolar potential. In principle, microinstabilities might be driven by temperature anisotropy, flows, or D-T non-thermal-equilibrium features. Hence, the possibility of microinstabilities deserves more investigation. The additional collisionality afforded by the ion-electron collisions reduces the end losses, leading to 20% higher densities than in the base case, less cooling in Case 6, and higher fusion rates. The effective Knudsen number is not much changed from that in the base case, and the KL effects on $f(v_z)$ are weaker in Case 6.

Fusion alphas at 0.001 concentration relative to the deuterium and tritium, ion-ion collisions with the fusion alpha particles, and ion-electron collisions are included in Case 7. The rationale for this choice of density of the alphas derives from consideration of the fusion reaction rates in the base case. We convert the kinetic fusion reaction rate in the base case to a reaction rate density and calculate the accumulated number density of reactions in ~5 ps to obtain an initial alpha particle density equal to $10^{21}/cm^3$. In addition, alphas are injected with the same type of planar source at z=0 as for the D-T ions using Eq.(2) for the rate consistent with an alpha particle density $10^{21}/cm^3$. The alphas slow on the electrons with rate ~10^{10} s^{-1} and collisionally exchange energy and momentum with the DT plasma. Over 30 ps the alphas slow on the electrons by ~30%. This corresponds to an energy loss to the plasma electrons ~10^{24} keV/cm^3, which is small compared to the electron energy density ~2x10^{25} keV/cm^3. In the simulation the temperature of the electron fluid is held fixed. Had we allowed the electrons to heat, there would have been electron energy transfer to the D-T ions because the deuterium-electron temperature equilibration rate is $\nu_\varepsilon^{i/e}$~3x$10^{10}s^{-1}$, and after 30 ps $\nu_\varepsilon^{i/e}\tau$~0.9 However, the alpha energy available is too small to substantially change the D-T temperatures over 30 ps. 10x longer times would be needed to produce enough alphas to heat the ions strongly. Nevertheless, the plasma ions are slightly hotter than in Case 1 due in part to direct

heating of the D-T by collisions with the alphas; and $<v_z>$ is 20% smaller with slightly less end loss and higher resulting plasma density. In consequence, the fusion reaction rates are 30% higher. The KL effects on $f(v_z)$ are slightly weaker in Case 7 than in Case 1.

In Case 8 we turned off ion-ion collisions in the D-T plasma. In this simulation the plasma streams collisionlessly to the absorbing boundaries. After a few transit times most of the $v_z<0$ ions have exited the system, and the ions injected by the planar source at $z=0$ fill the volume. $f(v_z)$ in the volume evolves asymptotically toward a half-Maxwellian with $v_z>0$ (but at 30 ps a remnant of the lowest velocity ions from the initial Maxwellian has not had sufficient time to transit the system and exit), and $<v_z>$ is approaching the expected analytical value $(2/\pi)^{1/2}v_{th}$. The end loss is higher than that for the collisional plasma in Case 1, and the average density is 20% lower. The average axial temperature in the mean drift frame is much reduced compared to that in Case 1 because of the partitioning of the axial kinetic energy between the substantial mean drift kinetic energy and the axial temperature, while the perpendicular velocity distribution is a Maxwellian with its 9 keV temperature dictated by the source. In consequence if the lower densities and composite temperature, the fusion rate is reduced relative to Case 1. The plasma density, axial flow, and axial temperature gradients are finite and qualitatively similar to those in Case 1. The perpendicular temperature profile in space is relatively flat.

In Cases 9 and 10 initial and source temperatures were varied, 2 keV and 12 keV, respectively. Along with Cases 1 and 2 this completes a limited scan in temperatures with completely absorbing boundary conditions: T_1 (keV) = [2, 4, 9, 12] with source injection rates given by Eq.(2) resulting in densities and collisionalities such that the corresponding Knudsen numbers using the volume-averaged densities and temperatures T_2 at 30 ps span almost two orders of magnitude: $N_k(<n>,<T_2>)$= [0.0047, 0.024, 0.11, 0.19]. The volume-averaged fusion reaction rates are a strongly increasing function of temperature and are again well matched by the thermal Maxwellian fusion rates using the local densities n and local temperatures T_2 (Fig. 8b). However, we observe that the ratios of the resulting kinetic fusion rates to the thermal Maxwellian fusion rates using the local densities and the initial/source temperature T_1 are limited to a relatively narrow range of values (Fig. 8a). Although the thermal Maxwellian fusion rates based on the initial and source temperature T_1 are not as physically relevant as using the actual plasma

temperature T_2, we use the fusion rates based on T_1 to compare to the linearized kinetic calculations in Ref. 4. We extract the calculated slab fusion reductions for temperatures T_1 (keV) =[2, 4, 9] and the representative Knudsen numbers plotted in Fig. 5 of Ref. 4, and display them in Fig. 8a. The particle simulation results for the fusion reductions at the two lowest values of N_k in Fig. 8a are lower by ~30% than the fusion reductions in Ref. 4, while the simulation fusion reductions are in closer agreement with those in Ref. 4 at N_k~0.1 However, our simulations address a different model and solve a fully nonlinear collisional kinetic equation, so that any comparison and agreement with Ref. 4 may not be meaningful.

In Case 11 we increased the source injection rates for the deuterium and tritium in Eq.(2) by x1.66 to increase the plasma density in steady state. The volume-averaged deuterium and tritium densities at 30 ps were $0.87 \text{x} 10^{24}$ cm^{-3} and 0.78 $\text{x}10^{24}$ cm^{-3}, respectively. However, the average flow velocity at 30 ps increased to 4.7 $\text{x}10^{7}$cm/s, and the ion temperatures were a little less than the base case. The kinetic fusion rate was increased at steady state, but still agrees well with the thermal Maxwellian fusion rate using the local densities and temperatures.

Table 1. Suite of simulations for 30 ps

Case/Run Nos.	Description and Comments
1/107	**Base Case**: 9 keV initial and source plasma; no reflection at right side; D-D, T-T, and D-T collisions; no electric fields; no ion-electron collisions
2/108	**Variation from base case**: 4 keV intial and source plasma **Results**: Colder, more collisional, much less fusion, similar density, lower axial drift velocity, much weaker Knudsen-layer (KL) effect on $f(v_z)$
3/110	**Variation from base case**: 50% reflectivity from right side boundary (9 keV retherm) **Results**: A little colder but higher density, particularly near reflecting wall; slightly more fusion, weaker drift velocity, less end loss, much weaker KL effect on $f(v_z)$
4/116	**Variation from base case**: 50% reflectivity from right side boundary (4 keV retherm) **Results**: Colder, more collisional, much less end loss, and denser than 107 and 110; little or no KL effect on $f(v_z)$
5/117	**Variation from base case**: Adds fully ionized Cu at 0.001× number density of D & T **Results**: More collisional; smaller N_k; slightly higher density because end loss smaller; more fusion; weaker KL effect on $f(v_z)$
6/118	**Variation from base case**: Adds ion-electron collisions and ambipolar electric field, T_e=9 keV **Results**: Slightly higher density and temperature; lower drift velocity and less endloss; so more fusion; KL modification of $f(v_z)$ is much weaker
7/114	**Variation from base case**: Adds fusion alpha particles at 0.001× number density of D & T and ion-electron collisions (but electron fluid temperature held constant) **Results**: Lower drift velocity and less end loss, so slightly higher density; slightly hotter plasma; 20% more fusion; alphas contribute more collisionality; effective N_k is reduced leading to weaker KL effect on $f(v_z)$
8/119	**Variation from base case**: Collisionless plasma **Results**: Higher drift velocity ~$0.8v_{th}$; $f(v_z,v_\perp)$ determined by source; more end loss, so density is ~20% less and fusion is reduced; $f(v_z,v_\perp)$ loses most $v_z<0$ particles
9/125	**Variation from base case**: 2 keV intial and source plasma **Results**: Colder, more collisional, much less fusion, higher density, much lower axial drift velocity, very small Knudsen-layer (KL) effect on $f(v_z)$
10/126	**Variation from base case**: 12 keV intial and source plasma **Results**: Hotter, less collisional, similar density, more fusion, higher axial drift velocity, strong Knudsen-layer (KL) effect on $f(v_z)$
11/131	**Variation from base case**: increased source rate, x1.66 **Results**: Higher axial drift velocity, slightly colder, higher density, more collisional, more fusion, strong Knudsen-layer (KL) effect on $f(v_z)$

Table 2. Fusion reaction rates, temperatures, $\langle v_z \rangle$, and N_k for suite of simulations

Case/Run Nos.	**Avg. kin Fusion**	**Kin/Maxw Fusion T_1**	**Kin/Maxw Fusion T_2**	T_z (keV)	$T_\perp$ (keV)	$\langle v_z \rangle$ (cm/s)	N_k	**KL $f(v_z)$**
1/107 (base)	5.46e13	0.568	0.927	7.0	7.8	3.0e7	0.11	Yes
2/108	4.14e12	0.573	0.935	3.5	3.6	1.6e7	0.024	Weaker
3/110	6.31e13	0.454	1.32	6.7	6.2	8.5e6	0.067	Weaker
4/116	3.19e13	N/A	1.45	4.6	4.3	1.2e7	0.031	No
5/117	6.20e13	0.585	0.938	7.0	7.9	3.0e7	0.075	Weaker
6/118	1.04e14	0.698	0.920	8.0	8.3	1.7e7	0.10	Weaker
7/114	6.91e13	0.606	0.934	7.3	7.9	2.4e7	0.097	Weaker
8/119	4.42e13	0.575	1.12	3.4	9.0	4.9e7	∞	No
9/125	4.85e11	0.717	1.05	1.9	1.9	7.5e6	0.0047	No
10/126	1.06e14	0.584	0.926	9.5	10.2	4.7e7	0.19	Yes
11/131	8.70e13	0.475	0.920	6.5	7.5	4.7e7	0.078	Yes

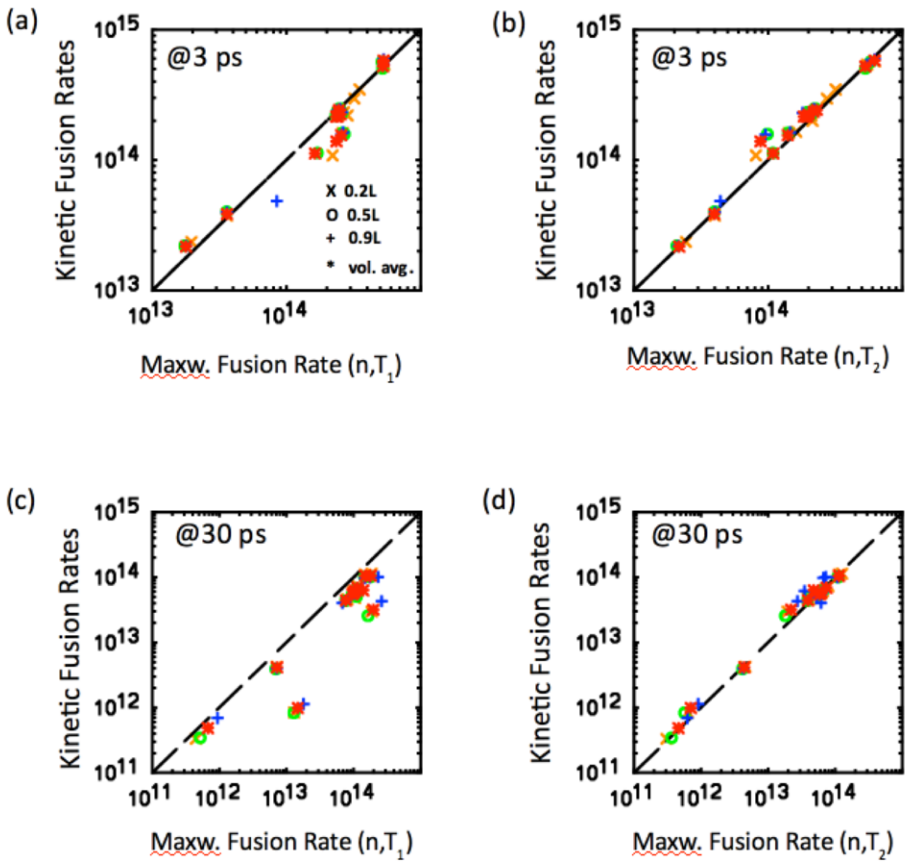

Figure 7. Kinetic fusion rates computed in the simulations plotted vs. thermal Maxwellian fusion rates using the local densities in the simulation and either the initial and source temperature T_1 or the local temperature in the simulation T_2 defined in Eq.(1) at 3 ps and 30 ps. Local fusion rates at z=0.2L, 0.5L, and 0.9L, and the volume averaged fusion rates are plotted.

IV. CONCLUSIONS

The particle simulations presented here are used to explore Knudsen-layer effects on D-T fusion in a one-dimensional system with a plasma source at z=0 and an absorbing boundary at z=L. Ion-ion collisions are included, and a combination of collisional diffusion and ballistic and hydrodynamic motion of the plasma determine the evolution of the plasma density, axial drift, temperature profiles, and end losses to the absorbing boundaries. The more energetic ions stream faster, are less collisional, and diffuse faster than do the colder ions. Loss of energetic ions to the absorbing walls contributes to cooling of the plasma. Interplay of the plasma sources, end losses to the absorbing walls, and hydrodynamic effects lead to decreases in the ion densities and temperatures. At

early times there are transients including rarefactions that also can contribute to cooling of the bulk plasma. The particle and hydrodynamic simulations show that in steady state the plasma density, temperature and pressure decrease away from the plasma source toward the absorbing boundary at $z=L$, while the plasma flow velocity increases away from the plasma source. The perpendicular and parallel ion temperatures generally evolve to an anisotropic state. The fusion depends on

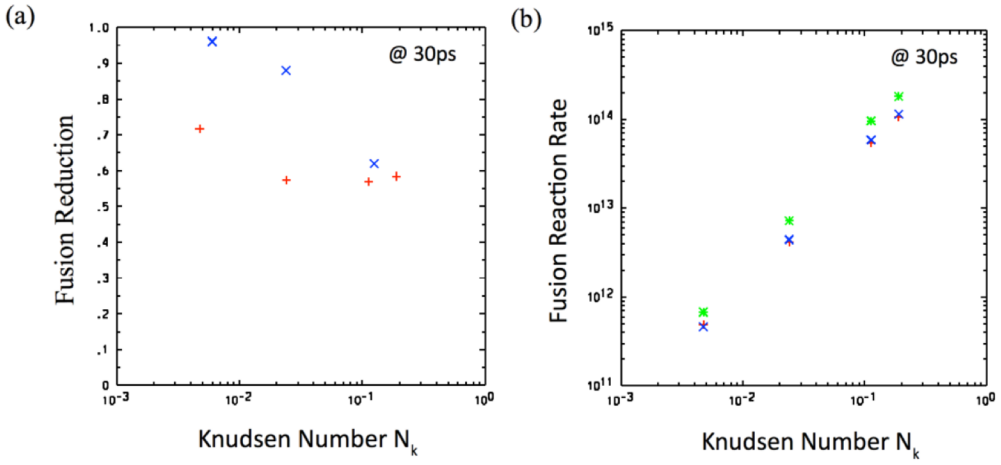

Figure 8. For plasma temperatures T_1 (keV) = {2, 4, 9, 12} (a) ratios of volume-averaged kinetic fusion rates to thermal Maxwellian fusion rate using local densities and intitial/source temperatures from the simulations (+) vs. $N_k(<n>,<T_2>)$ and fusion reduction fraction (x) from Ref. 4 vs. $N_k(n_0,T_0)$ and (b) volume-averaged fusion reaction rates (+ kinetic fusion rate, x thermal Maxwellian fusion rate using local ion densities n and temperature T_2, * thermal Maxwellian fusion rate using local ion densities n and initial/source temperature T_1) for a scan of Knudsen numbers $N_k(<n>,<T_2>)$.

the product of the D-T densities and strongly on the energy content of the D-T velocity distributions relative to the average mass motion (the fusion cross-section steadily increases with increasing energy up to ~70 keV). The fusion reaction rates decrease with decreasing ion density and temperature. Thus, the fusion reactivities are reduced relative to the thermal Maxwellian fusion reactivities computed for initial and source plasma temperatures at the local densities in the simulations; and although the reductions are significant, the relative reductions vary in a limited range as a function of temperature T_1 and Knudsen number N_k.

Our simulations exhibit Knudsen-layer deformations of the velocity distributions. Nevertheless, the thermal Maxwellian fusion reaction rates are a good estimator of the kinetic fusion reaction rates in the simulations if one uses the local plasma densities and the local temperatures defined in Eq.(1) because the KL deformations to the velocity distributions occur at higher energies than the Gamow peak and the energy interval that dominates the contributions to the fusion reactivity.

The simulation results indicate that the interplay between the plasma source and the absorbing walls, ion collisions, and temperature cooling accompanying increased mass motion and end losses are the dominant factors in influencing the fusion reaction rates in the scenarios studied here. The comparison of the kinetic fusion reaction rates to the thermal Maxwellian reaction rates using the local density and temperatures T_2 is more meaningful than comparisons to thermal reaction rates using T_1 and shows relatively good agreement over the range of parameters consider here. The results here generally suggest that hydrodynamic effects are dominant and that the Knudsen-layer effects are sub-dominant in influencing fusion rates for the model problem and range of parameters considered.

We thank H. Whitley, J. Greenough, F. Graziani, D. Ryutov, K. Molvig, and B. Albright for useful suggestions, insights, and encouragement. We also thank R. Procassini for developing his particle code ICEPIC and making it available. This work was performed under the auspices of the U. S. Department of Energy by the Lawrence Livermore National Laboratory under Contract DE-AC52-07NA27344.

References

[1]D. B. Henderson, Phys. Rev. Lett. **33**, 1142 (1974).

[2]A. G. Petschek and D. B. Henderson, Nucl. Fusion **19**, 1678 (1979).

[3]K. Molvig, N. Hoffman, B. J. Albright, E. M. Nelson, and R. B. Webster, Phys. Rev. Lett. **109**, 095001 (2012).

[4]B. J. Albright, K. Molvig, C.-K. Huang, A. N. Simakov, E. S. Dodd, N. M. Hoffman, G. Kagan, and P. F. Schmit, Phys. Plasmas **20**, 122705 (2013).

[5]H.-S. Bosch and G. M. Hale, Nucl. Fusion 32, 611 (1992).

[6]S. Atzeni and J. Meyer-ter-Vehn, *The Physics of Inertial Fusion: Beam Plasma Interaction, Hydrodynamics, Hot Dense Matter* (Oxford Science Publications, June 2004), Sec. 1.4.

[7]R. Hockney and J. Eastwood, *Computer Simulation Using Particles* (McGraw-Hill, New York, 1981).

[8]C. K. Birdsall and A. B. Langdon, *Plasma Physics via Computer Simulation* (McGraw-Hill, New York, 1985).

[9]T. Takizuka and H. Abe, J. Comput. Phys. **25**, 205 (1977).

[10]K. Nanbu, Phys. Rev. E **55**, 4642 (1997).

[11]R. J. Procassini, Ph. D. Thesis, Univ. of California Berkeley, 1990. ICEPIC derived from the TESS particle code developed by R. J. Procassini and B. I. Cohen; R.J. Procassini, C.K. Birdsall, B.I. Cohen, Nuc. Fusion **30**, 2329 (1990); R. J. Procassini and B. I. Cohen, J. Comp. Phys. **102**, 39 (1992).

[12]D. S. Lemons, D. Winske, W. Daughton, and B. J. Albright, J. Comput. Phys. **228**, 1391 (2009).

[13]B. I. Cohen, A. M. Dimits, A. Friedman, and R. E. Caflisch, IEEE Trans. Plasma Sci. **38**, 2394 (2010).

[14]P. E. Kloeden and E. Platen, *Numerical Solution of Stochastic Differential Equations* (Springer-Verlag, Berlin, 1999).

[15] L. D. Landau and E. M. Lifshitz, *Statistical Physics*, *Part 1*, (Pergamon, Tarrytown, NY, 1980), p. 544; J. A. Newbury, C. T. Russell, and G. M. Lindsay, Geophys. Research Lett. **24**, 1431 (1997).

[16]G. B. Zimmerman and W. L. Kruer, Comments on Plasma Physics and Controlled Fusion 2, no. 2 (1975): 51-61.

[17]R. C. Bissell and P. C. Johnson, Phys. Fluids **30**, 779 (1987); S. E. Parker, R. J. Procassini, C. K. Birdsall, and B. I. Cohen, J. Comput. Phys. **104**, 41 (1993).